Carbon nitride coupled with carbon nanohorns for improved photocatalytic hydrogen production and dyes degradation

Eirini-Olga Alexandridou[a], Maria Anagnostopoulou[b], Elton M. Dias[c,d], Zois Syrgiannis[e,f], Valerie Keller[b], Camille Petit[c], Konstantinos C. Christoforidis[a,b,c,*]

[a] Department of Environmental Engineering, Democritus University of Thrace, Xanthi 67100, Greece

[b] Institut de Chimie et Procédés Pour l'Energie, l'Environnement et la Santé, (ICPEES) ECPM, University of Strasbourg, 25 rue Becquerel Cedex 2, Strasbourg, France

[c] Barrer Centre, Department of Chemical Engineering, Imperial College London, South Kensington Campus, London SW7 2AZ, U.K.

[d] Department of Chemical Engineering, Torrington Place, University College London, London, WC1E 7JE

[e] Department of Chemistry, Northwestern University, Evanston, Illinois 60208, USA

[f] Simpson Querrey Institute, Northwestern University, Chicago, Illinois 60611, USA

* Corresponding author email: kochristo@env.duth.gr

Abstract

In the present study we attempted to develop photoactive nanocomposites via the facile coupling of carbon nitride (CN) with single walled carbon nanohorns (CNHs). Photocatalytic activity was evaluated for the degradation of Rhodamine B (RhB) and the production of H_2. The CNHs content noticeably affected the photoactivity of the nanocomposites and the best performing material exhibited a 3-fold increase in photocatalytic H_2 production compared to pristine CN using 1 wt.% Pt as co-catalyst. A systematic study was undertaken to explain the mechanistic aspects of the photo-reaction process. The active species responsible for the photodegradation of RhB were identified using reference reactions. Such species were further studied using in-situ spin-trap EPR experiments. Photoluminescence and time-resolved fluorescence decay kinetics suggested faster transfer of photogenerated electron/hole pairs resulting in reduced charge recombination phenomena in the nanocomposites. The combined photocatalytic application and characterization of the prepared materials revealed that the promotion of the redox reactions in based on improvements on the charge separation efficiency.

Keywords: carbon nanostructures, carbon nanohorns, water splitting, hydrogen, dyes

1. Introduction

Over the last few years, significant efforts have been devoted to building an eco-friendly society. Although improvements have been made in this direction, there remain challenges in several areas. These include the sustainable production of carbon-free fuels and the development of sustainable processes for environmental cleaning-up. The first issue relates to the negative impact of fossil fuels usage on the environment via the release of greenhouse gases, the depletion of their reserves and the increasing global demand for energy. The second is linked to environmental pollution due to anthropogenic activities. For both issues, several strategies have been proposed. Among them, photocatalytic processes have gained increased attention [1-3]. Photocatalysis using semiconductor materials (SCs) has been used to produce hydrogen (H_2) either from water splitting or from photoreforming of oxygenates/carbohydrates [1, 2] and the degradation of organic pollutants from air or aqueous samples [3, 4]. H_2 is predicted to play a major role in the future as an energy carrier [1, 2, 5, 6] able to replace fossil fuels and has numerous industrial applications such as the synthesis of ammonia or oil refining. Producing H_2 from an environmentally-friendly process such as using water and renewable solar energy offers sustainability advantages.

There are several challenges and issues that must be overcome for this process to meet industrial standards. The most important aspect is the development of the photocatalyst. To this day, several materials have been exploited in both applications including oxides [4], sulphides [7], perovskites [8] and organic SCs [9, 10]. Among them, one should mention graphitic-like carbon nitride (CN), a visible light activated material with relatively low band gap energy (E_g of ~ 2.7 eV) which is considered a promising candidate as photocatalyst with a variety of applications [10-18]. The interest in CN originates from its intrinsic properties such as non-toxicity, low-cost, easy preparation protocols and high chemical and thermal stability [3, 16]. These characteristics meet the requirements for the practical application of a photocatalyst.

Nevertheless, one of the main drawbacks is the fast recombination rates of photogenerated charges that hinders photoactivity of bare CN [19]. Different strategies have been applied to mitigate this limitation including structure engineering [15, 20, 21], defects formation [22] and doping [23]. An added benefit of using CN is its polymeric nature that allows easy modifications. This feature has been utilized for the functionalization of CN with heterostructures and nanoparticles and the development of hybrids and heterojunctions mainly as a way to improve charge separation [12, 14, 16, 17, 24-27].

So far, a variety of materials has been coupled with CN including semiconductors for the development of heterojunctions [14, 26, 28], porous materials [16], conductive materials [29] or even insulators [12, 30]. Among them, of particular interest are carbon nanostructures like carbon nanotubes (CNTs) [24, 31, 32], reduced graphene oxide [17], graphene [29, 33], carbon dots [34, 35] or carbon units [25], carbon nanospheres [36] and carbon nanohorns (CNHs) [37]. CNHs are spherical clusters made of aggregates of single walled carbon nanocones [38]. Depending on the selected material, these nanostructures can allow the development of metal-free materials. Photoactivity either in H_2 production [24, 33, 35] or organic pollutants degradation [35, 36] improves significantly in such heterostructures owing to an efficient charge separation. The dimension of carbon nanostructures at the nanoscale plays vital role in photoactivity [24]. In particular, the wall thickness of CNTs controls the charge separation efficiency in CN/CNTs composites with single walled CNTs presenting the highest efficiency [24]. There are very few reports on the development of photocatalysts containing CNHs or nanocones [39-43] despite key advantages over CNTs, e.g. absence of metal catalysts in their synthesis and mass production at room temperature [38]. One of the critical properties of CNHs in photocatalytic systems is the ability to act as an electron-transfer media [44]. This allows CNHs to hinder recombination rates in composite materials [45] and improve photocatalytic efficiency.

Herein, we report the development of a new class of metal-free nanocomposite photocatalysts by coupling CN with single-walled CNHs through a solid-state thermal condensation reaction. The content of the CNHs was controlled in the final heterostructure and the materials were fully characterized. The photocatalytic activity was evaluated in H_2 production from water splitting and RhB degradation as a model organic pollutant. We show that CNHs have a positive effect on photoactivity that depends on the actual CNHs content. As is it demonstrated, the improved photocatalytic activity originates from the improvement in the electronic properties related with charge separation. To the best of our knowledge, CN/CNHs photocatalysts have never been tested in photocatalytic applications.

2. Experimental section

2.1. Materials synthesis

All chemicals were used as received without any further purification. Pure CN was synthesized via the thermal polycondensation of melamine (Aldrich) at 550 °C for 4 h with a heating rate of 3 °C min^{-1} [24]. For the synthesis of a series of CN/CNHs nanocomposites, melamine (Aldrich) was mixed with a specific amount of single-walled CNHs (Aldrich, Carbon Nanohorms, as grown). First, 10 g of melamine were sonicated at room temperature for 1 h in 400 mL of double distilled water. Then, a specific amount of bare CNHs was added and the dispersion was further sonicated for 3 h followed by stirring overnight at 80 °C. Four samples were developed by varying the CNHs content: 5, 10, 20 or 100 mg corresponding to a 0.05 %, 0.1 %, 0.2 % and 1.0 % by weight CNHs nominal content, respectively. The powders were collected by filtration, dried overnight at 70 °C and thermally treated at conditions identical as the bare CN sample. All as-prepared materials were grounded into powder, incubated under stirring with 0.1 M HNO_3 for 1 h, washed with double-distilled water and ethanol and dried

under vacuum at 90 ^{o}C overnight. Finally, the materials were immersed in DMSO for 4 days, collected via centrifugation at 12000 rpm for 30 min, washed with ethanol three times, dried at 70 °C overnight and vacuum treated at 90 °C overnight. All materials were grounded to fine powder using agate mortar. The developed nanocomposites are labeled NHCN*x* where the increasing *x* value denotes samples with increasing CNH content. CN stands for the as prepared carbon nitride catalyst.

2.2. Co-catalyst deposition

Pt nanoparticles, used as co-catalysts in the photocatalytic H_2 production process, were deposited on the surface of the catalyst to achieve 1 % Pt concentration by weight in relation to the photocatalyst, using H_2PtCl_6 (Aldrich) as precursor. First, the catalyst was suspended with the aid of sonication (10 min) followed by stirring for 30 min in double distilled water. Then, the proper quantity of H_2PtCl_6 was introduced followed by 5 min stirring. Chemical reduction for the production of Pt nanoparticles was performed by adding $NaBH_4$ (Aldrich) aqueous solution. The Pt:$NaBH_4$ molar ratio was kept at 1:5. The whole process was performed under argon flow to ensure the removal of air. The final solid was collected by centrifugation, washed three times with water, three times with ethanol, dried at 70 °C overnight and finally vacuum treated at 90 °C overnight.

2.2. Materials characterization

X-ray diffraction patterns were recorded with a PANalytical X'Pert PRO diffractometer operating at 40 kV and 40 mA using CuKα radiation (λ = 0.15418 nm). Nitrogen adsorption-desorption isotherms were obtained at 77 K using a Micromeritics 3Flex apparatus. Prior to analysis materials were degassed for 24 h at 120 °C at 0.2 mbar pressure. They were then degassed in situ on the porosity analyzer for 6 h down to approximately 0.0030 mbar. Specific surface area was determined using the Brunauer-Emmett-Teller (BET) model [46]. Attenuated

total reflection Fourier transform infrared (ATR-FTIR) spectra were collected using a PerkinElmer Spectrum 100 Spectrometer on the as-synthesised samples. The spectra were collected 8 times with a resolution of 1 cm^{-1}. Thermogravimetric analysis (TGA) was performed with a Netzsch TG 209 F1 Libra instrument from 100 °C to 900 °C at a heating rate of 10 °C min^{-1} and under nitrogen flow (100 mL min^{-1}). UV-vis diffuse-reflectance spectra were collected with a Shimadzu UV2100 apparatus using Teflon as reference. Transmission electron microscopy (TEM) images were taken with a JEOL 2100Plus instrument. Materials were sonicated in ethanol and then drop casted on a carbon coated copper grid. A Fluorolog FM-32 spectrofluorometer (Horiba Jobin Yvon) was used to acquire the static photoluminescence spectra. Fluorescence intensity decay curves were acquired with a time-correlated single photo counting (TCSPC) setup (DeltaFlex, Horiba). Pulsed 404 nm excitation (10 kHz repetition rate) was generated by a laser diode and fluorescence was detected at 455 nm (SPC-650 detector, Horiba). An X-band Bruker ER200D Electron Paramagnetic Resonance (EPR) spectrometer was used to perform spin trap experiments. The 5,5-dimethyl-1-pyrroline N-oxide (DMPO) was used as spit trap for the detection of superoxide anion radicals ($O_2^{\bullet -}$) and hydroxyl radicals ($OH^{\bullet}$) at room temperature. A quartz EPR flat cell was used.

2.3. Photocatalytic activity evaluation

2.3.1. Degradation reactions

The photocatalytic activity of the prepared materials was evaluated for the degradation of rhodamine B (RhB) in aqueous solutions using Milli-Q water. Catalytic tests were performed using a xenon arc lamp (150 W, $\lambda > 325$ nm, LOT Quantum Design) equipped with a water filter. Reactions under pure visible light irradiation were conducted using a 400 nm cut-off filter. Prior to irradiation, the catalyst suspension was incubated with the organic pollutant for 1 h in the dark to ensure adsorption/desorption equilibrium. The catalytic results reported

herein are after adsorption/desorption equilibrium was reached. Aliquots were sampled periodically and filtered through a 0.2-μm PTFE syringe filter. A PerkinElmer (Lamda 35) UV-Vis spectrophotometer was used to determine the concentration of the pollutants. In all catalytic tests, the catalyst concentration was 0.8 g L^{-1}. 10 mg L^{-1} and 5 mg L^{-1} of the organic substrate were used for experiments performed under UV-Vis and pure visible light irradiation, respectively. Catalytic tests were performed in triplicate. To study the stability of the catalysts, recycling experiments were conducted by collecting the catalyst through filtration, washing it three times with 100 mL of water and once with 50 mL of acetone. Finally, the catalyst was dried at 100 °C overnight under vacuum. To identify the reactive species responsible for the degradation reaction, reference reactions were contacted using scavengers. As hole (h^+) and hydroxyl radical ($OH^{\bullet}$) scavengers, triethanolamine (TEOA, Aldrich) and *tert*-butyl alcohol (TBA, Aldrich) (0.1 mmol) were used, respectively. A reference reaction under saturated nitrogen atmosphere was performed to study the effect of $O_2^{\bullet-}$ formation. In this reaction, the reaction mixture was purged with N_2 gas for 30 min in dark conditions before turning on the light. N_2 flow was maintained after initiating the reaction to ensure anaerobic conditions throughout the reaction.

2.3.2. Photocatalytic H_2 production

Photocatalytic hydrogen production was evaluated under pure visible light irradiation (420 nm) using a 300 W Xe lamp (LOT Quantum Design) under flow reaction conditions. A liquid/solid Teflon-lined stainless still reactor was used. 30 mg of the catalyst were suspended into 40 mL of a 10 % by volume of triethanolamine (TEOA, Aldrich) aqueous solution. An argon flow of 10 mL min^{-1} was used to remove air from the reaction mixture and the reaction temperature was maintained at 24 °C using a cryostat. Evolved gases were analysed on-line using a GC/TCD (Agilent Technologies) with hayesep and molecular sieve packed columns in series using Ar as gas carrier. Photocatalytic H_2 evolution was monitored for 6 h. Recycling

187 experiments were conducted by collecting the used catalyst through filtration and washing it
188 with 100 mL of water (three times) and 50 mL of acetone before drying at 100 °C overnight
189 under vacuum.

190

3. Results and Discussion

3.1. Catalysts characterization

Quantification of the CNHs content in the final material was performed by means of thermogravimetric analysis (TGA). The TG profiles of all materials are presented in Figure S1. The CNHs content was calculated by the remaining weight at 800 ^{o}C. Decomposition of CN began at temperature around 600 ^{o}C. The CNHs content derived from TGA are given in Table 1. For all nanocomposites, the amount of CNHs content in the final material was significantly higher than the nominal amount used during the synthesis. This probably originates from the mass loss of melamine during the thermal polycondensation process as evidenced by the approximately 48 % yield of the pure CN synthesis.

Table 1. CNHs content in the nanocomposites as derived from TGA and BET surface areas of all the materials derived from N_2 sorption analyses at 77 K.

Sample	CNHs content (wt.%)	BET surface area (m^2 g^{-1})
CN	–	5.3
NHCN1	0.5	5.1
NHCN2	0.8	5.0
NHCN3	2.1	10.6
NHCN4	5.2	17.2

The structure and chemical features of the bare and CNHs functionalized CN were studied using XRD and ATR spectroscopy. Figure 1A presents the XRD patterns of the materials. The two reflections characteristic of the CN structure appeared in all samples. The low-angle diffraction peak positioned at approximately 13.0^{o} 2θ corresponds to the (100) crystal plane of

CN and the one at 27.3° 2θ to the (002), the interplanar distance between sheets [13, 47]. These two features confirmed the successful formation of CN.

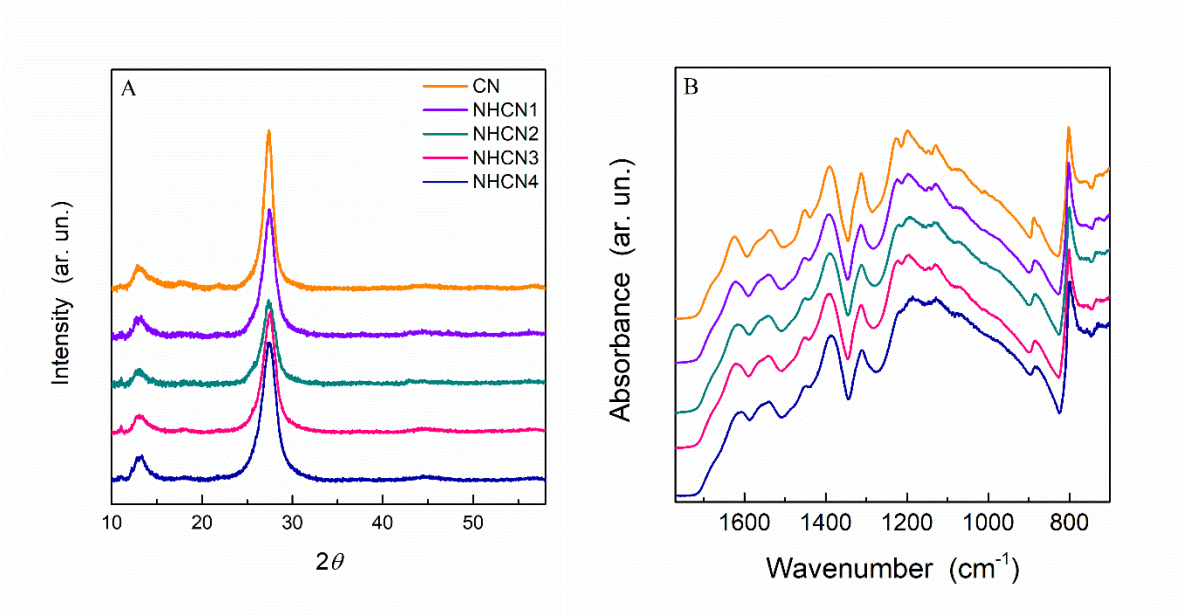

Figure 1. XRD patterns (A) and ATR spectra (B) of CN and the NHCNx nanocomposites with varying CNHs contents.

Figure 1B displays the ATR-FTIR spectra of all samples prepared. Full scale spectra are given in Figure S2. All the characteristic vibrational modes of carbon nitride were detected in the bare CN and the NHCN*x* series without any obvious difference between the prepared samples [13, 15]. The multiple bands in the 1200 cm^{-1} to 1680 cm^{-1} region originate from the C—N stretching and bending vibrations in N-heterocycles[13, 15]. The sharp band at 800 cm^{-1} is ascribed to the breathing mode of the triazine units[13, 15]. The broad band in the 3200 cm^{-1} region is due to the stretching vibration of N—H bonds (primary and secondary amines) [15]. The unchanged features in the NHCN*x* series compared with the bare CN provides evidence

223 that the chemical moieties of CN remained unaltered when the synthesis was performed in the
224 presence of CNHs.

225 Further evidence on the formation of the layered CN structure were obtained with TEM
226 analysis. Figure 2 presented representative TEM images of CN and the NHCN2
227 nanocomposite. The typical platelet-like structure of CN was detected for both materials. The
228 CN sample presented a smooth surface while NHCN2 exhibited CNHs spherical structures
229 (highlighted with arrows) with dimensions ranging from 50 nm to 80 nm in diameter [41, 48].
230 These results indicated that CNHs structure is not affected by the synthesis process applied for
231 the development of the nanocomposites as in the case of the TiO_2/CNHs nanohybrids [49, 50].
232 It is highlighted that the samples for TEM analysis were sonicated for 15 min prior to
233 deposition. Therefore, the presence of CNHs on the surface of the layered CN structure
234 suggests that the developed nanocomposites are stable, and the two phases interact strongly.

235

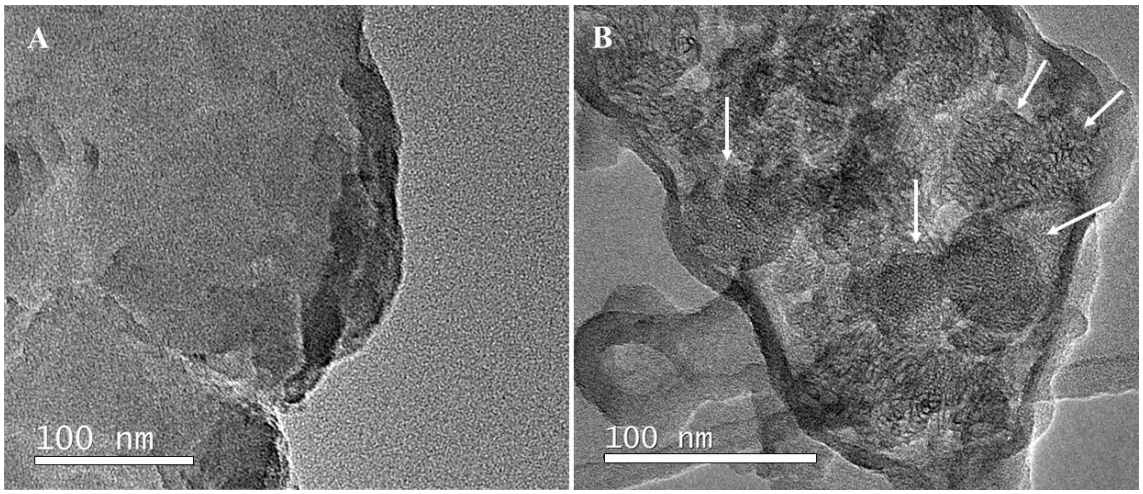

236

237 **Figure 2.** TEM images of CN (A) and the NHCN2 nanocomposite (B).

238

Since the efficiency of a heterogeneous catalyst depends greatly on the surface area, N_2 adsorption/desorption isotherms were performed to determine the BET specific surface (Table 1). The corresponding N_2 adsorption/desorption isotherms are given in Figure S3. No differences were detected between CN and the nanocomposites with low CNHs contents (i.e. NHCN1 and NHCN2). However, the surface area increased for the nanocomposites with higher CHNs contents. Nevertheless, in all cases, the surface area remained low. This is to be expected taking into account the low amount of CNHs used for the preparation of the nanocomposites as well as the fact that in CNHs, the nanocones are assembled through the open tips forming spherical clusters [38].

3.2. Photocatalytic activity

3.2.1. Photodegradation reactions

The photocatalytic activity of the prepared materials in organic pollutants degradation was tested against the removal of RhB. Figure 3A presents the time-dependence of RhB degradation under UV-Vis irradiation. First, we observed an evident increase in photoactivity for the nanocomposites with low CNHs content compared to CN. In the nanocomposite series, photoactivity decreased with increasing CNHs content. The NHCN1 and NHCN2 catalysts presented approximately similar photoactivity with efficiency approaching 100 % within 1 h of irradiation while NHCN4 was less active than CN. More importantly, under visible light only, the NHCN1 nanocomposite was proven active (Figure 3B) and performed better than the CN catalyst.

To test the stability of the prepared materials, we conducted recycling experiments on the most active catalyst, i.e. NHCN1. No apparent deactivation of the catalyst was observed after four consecutive cycles. The efficiency of the reused catalyst is reported for 0.5 h and 1 h reaction

time in Figure 3C. These data demonstrate the stability of the prepared nanocomposites under the catalytic conditions applied. Post-characterization of the NHCN1 used catalyst with ATR-FTIR further established the stability since no obvious differences were observed compared with the fresh catalyst (Figure S4).

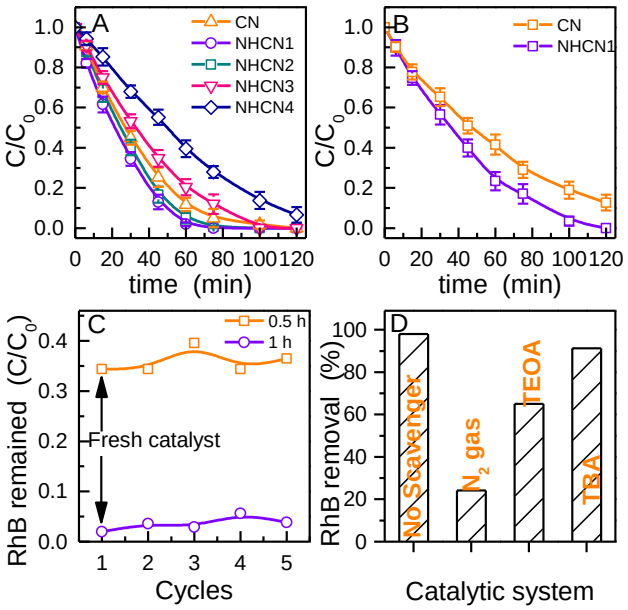

Figure 3. A) Time evolution of RhB photocatalytic degradation using CN and the nanocomposite photocatalysts under UV-Vis irradiation. B) Time evolution of RhB photocatalytic degradation using CN and NHCN1 under pure visible light irradiation (> 400 nm). C) RhB degradation efficiency after 0.5 h and 1 h under UV-Vis irradiation for five consecutive reaction processes using the NHCN1 photocatalyst. D) Effect of various scavengers (no scavenger, nitrogen gas, TEOA and TBA) on RhB degradation efficiency under 1 h UV-Vis irradiation using the NHCN1 photocatalyst.

3.2.2. Photocatalytic hydrogen production

The photocatalytic activity of the prepared materials was further evaluated for H_2 production from water splitting. For all materials tested in H_2 production, Pt (1 wt.%) was used as co-catalyst. Figure 4 compares the photocatalytic H_2 production rates of the reference CN-Pt and the NHCN1-Pt and NHCN2-Pt nanocomposites under pure visible light irradiation (> 420 nm), where Pt at a 1 wt.% was used as cocatalyst. Photocatalytic tests were performed under flow conditions (Ar flow) and H_2 evolution was monitored for a period of 6 h. All materials tested presented steady H_2 production rates within this period. This observation demonstrated the stability of the prepared materials under working conditions. As in the case of the photodegradation reactions, the nanocomposites presented superior photoactivity in H_2 evolution reaction compared to the reference CN sample. Under identical condition, NHCN1-Pt showed an impressive 3-fold increase in H_2 production rate compared to CN-Pt. Increase of the CNHs content decreased H_2 evolution (Figure 4), as observed for the RhB degradation reaction. Nevertheless, the NHCN2-Pt nanocomposite presented much higher H_2 evolution rate than CN-Pt. It is highlighted that no H_2 was produced when the prepared materials were tested without the presence of Pt as co-catalyst. Finally, the nanocomposite catalysts showed excellent stability with no apparent deactivation under the catalytic conditions applied as demonstrated by the consecutive experiments (recycling reactions R1-R3) presented in Figure 4. An additional important information extracted from the H_2 evolution reaction performed under pure visible light irradiation is that the performance in RhB degradation with light-irradiation of > 400 nm is based on the activity of the photocatalysts and not on dye-sensitization effects. Indeed, dye sensitization effects are not expected in the H_2 evolution reaction under the conditions applied herein.

303 To establish the possible contribution of the nanocomposite formation on its photocatalytic
304 activity, we prepared and tested a physical mixture of CN and CNHs (labelled PM) using the
305 mass ratio of NHCN1. The activity of the physical mixture matched that of CN. This indicated
306 that the conditions applied for the synthesis offered the development of a synergy between the
307 two phases that is not present in a physical mixture. Considering the unchanged specific surface
308 area between CN reference and the nanocomposites NHCN1 and NHCN2, the enhanced
309 photocatalytic H_2 production of the nanocomposites suggests a synergy and an interaction
310 between the CN and the CNHs phases, which induced changes in optical and electronic
311 properties. Improvements in light absorption as well as the presence of an optical charge
312 transfer transition have been observed in composites made through the coupling of SCs with
313 carbon matrixes including carbon nanostructures [24, 43, 51]. To examine the presence of such
314 contributions, we investigated the optical and electronic properties of the prepared catalysts.

315

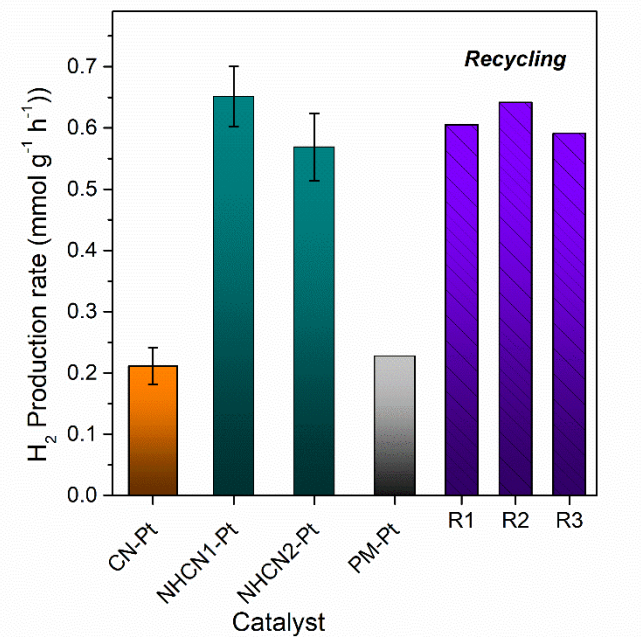

316

317 **Figure 4.** Photocatalytic H_2 production using the bare CN-Pt and the NHCN1-Pt and NHCN2-
318 Pt nanocomposites under pure visible light irradiation (> 420 nm). 1 wt.% Pt was used as

cocatalyst. The recycling reactions (R1-R3) displayed on the right side of the panel correspond to the NHCN1 nanocomposite. PM refers to a sample based on a physical mixture.

3.3. Photocatalytic mechanism and optoelectronic properties

Reference reactions using scavengers were performed to get insights into the photocatalytic reaction mechanism and identify the active species that contribute to RhB degradation. In these control experiments, we used the most active catalyst, i.e. NHCN1. TBA and TEOA and were employed as hydroxyl radicals ($OH^{\bullet}$) and hole (h^{+}) scavengers, respectively. A reference reaction under saturated N_2 atmosphere was contacted to evaluate the contribution of superoxide anion radicals $O_2^{\bullet-}$. The catalytic data are given in Figure 3D. TBA did not affect significantly the removal of RhB suggesting that $OH^{\bullet}$ had little effect in the reaction mechanism. These results were not surprising since the oxidation potential of VB h^{+} in CN (~1.6 eV) [52] is not positive enough to oxidize either OH^{-} (1.99 eV) or adsorbed water molecules (2.37 eV) [9, 14, 53]. Degradation efficiency was supressed in the presence of TEOA. This indicated that h^{+} have a role in the removal of RhB using the NHCN1 nanocomposite. However, the efficiency decreased when the reaction was performed under saturated N_2 atmosphere. Based on the energy level of the CB in CN (~ −1.1 eV) [9, 14, 52], photogenerated CB e^{-} in CN can reduce O_2 and form $O_2^{\bullet-}$, since the standard redox potential of $O_2/O_2^{\bullet-}$ is -0.046 eV *vs*. NHE. These results indicated that h^{+} and $O_2^{\bullet-}$ are the active species that participate in the degradation of RhB with $O_2^{\bullet-}$ being the dominant species that control activity. The small contribution of $OH^{\bullet}$ in the catalytic mechanism could be assigned to the production of $OH^{\bullet}$ via O_2 multi-electron reduction process and the production of H_2O_2 [14, 52, 54]. These results are in line with recent studies in pristine and modified CN photocatalysts [12, 14, 23, 55, 56]. To further verify the formation of $O_2^{\bullet-}$, in-situ EPR experiments [57] were conducted

using DMPO as spin trap. Using a suspension of NHCN1 in methanol, we observed the characteristic pattern of the DMPO-$O_2^{\bullet-}$ spin adduct under 10 min of pure visible light irradiation (Figure 5, upper spectrum). Performing the same experiment in aqueous NHCN1 suspension, we detected an EPR signal with a 1:2:2:1 intensity ratio corresponding to the DMPO-$OH^{\bullet}$ spin adduct (Figure 5, lower spectrum). However, the signal intensity of the latter was significantly weaker than that of the former. These EPR results verified the catalytic reactions performed in the presence of scavengers and further established $O_2^{\bullet-}$ as the main active species of the nanocomposites in the photodegradation reaction.

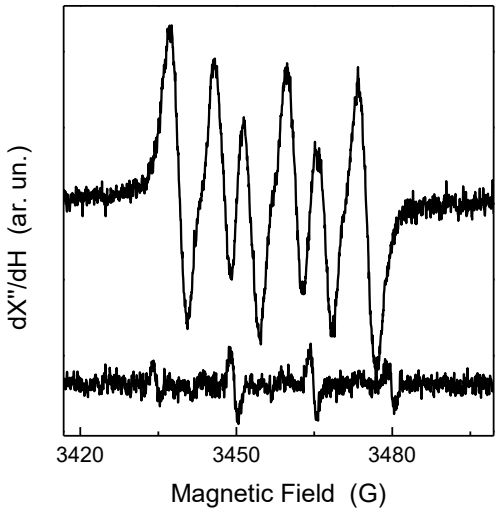

Figure 5. Room temperature DMPO spin-trapping EPR spectra of the NHCN1 nanocomposite in methanol suspension (upper spectrum) and in aqueous suspensions (lower spectrum) under 10 min visible light irradiation.

We evaluated the optical absorption properties of the prepared materials using DR-UV-Vis spectroscopy (Figure S5). The absorption edge of CN and the NHCN*x* nanocomposites was

approximately positioned at 450 nm, which corresponds to a band gap energy of ~2.8 eV [9, 15]. In addition, the presence of CNHs induced an increase in the absorption of the entire visible region. This was obvious even for the nanocomposite with the lowest CNHs amount. The absorption increased with increasing CNHs content and was strictly related with the presence of CNHs [24]. These changes in the visible region of the UV-Vis spectra have been previously observed in similar nanocomposites containing carbon nanostructures [17, 24, 25]. Bearing in mind that CNHs are not photoactive, the significantly increased visible light absorption of the nanocomposites with high CNHs content may indicate overloading of the CN with CNHs. Overloading could have a negative impact on photoactivity by reducing the accessibility to light of some CN particles. This could explain the reduced activity of the nanocomposites with high CNHs content (Figure 3A).

Photoluminescence (PL) emissions originating from the radiative recombination of free charge carriers can be used to evaluate charge separation efficiency in photoactive materials [12]. PL emission spectra of the bare CN and the NHCN1 nanocomposite are given in Figure 6A. As evidenced, the PL emission intensity is significantly decreased in the nanocomposite compared with the CN sample. The coupling of carbon nanostructures with TiO_2 [42, 43] and other SCs [24, 41] for the development of nanocomposites can improve charge carrier separation of photo induced e^-/h^+ pairs and supress the charge recombination phenomena resulting in a decrease of the PL intensity. Further insight into the photoinduced charges was obtained by time-resolved fluorescence decay kinetics recorded with TCSPC at the corresponding steady-state emission peaks (Figure 6B). The NHCN1 sample presented decreased emission lifetime compared to CN. This observation, combined with the quenching of the emission intensity, indicates that the presence of CNHs in the nanocomposite introduced an additional decay pathway in kinetic competition with radiative recombination [58, 59]. This result suggests enhanced singlet exciton dissociation in the nanocomposite accelerating charge transfer [60-62]. Considering

384 that CNHs did not alter the CN structure (i.e. interlayer distance), the observed decreased
385 lifetime could originate from the transfer of photogenerated e^- in the conduction band of CN to
386 CNHs preventing a direct recombination of photoexcited e^- and h^+ [63]. Charge transfer of
387 photoinduced electrons to and from CNHs has been demonstrated in composites containing
388 CNHs [44]. In this way, the fast recombination rates of photogenerated charges in CN, i.e. the
389 main drawback of using CN in photocatalysis, is overcome and the nanocomposites present
390 enhanced photoactivity in both photodegradation reactions and water splitting process.

391

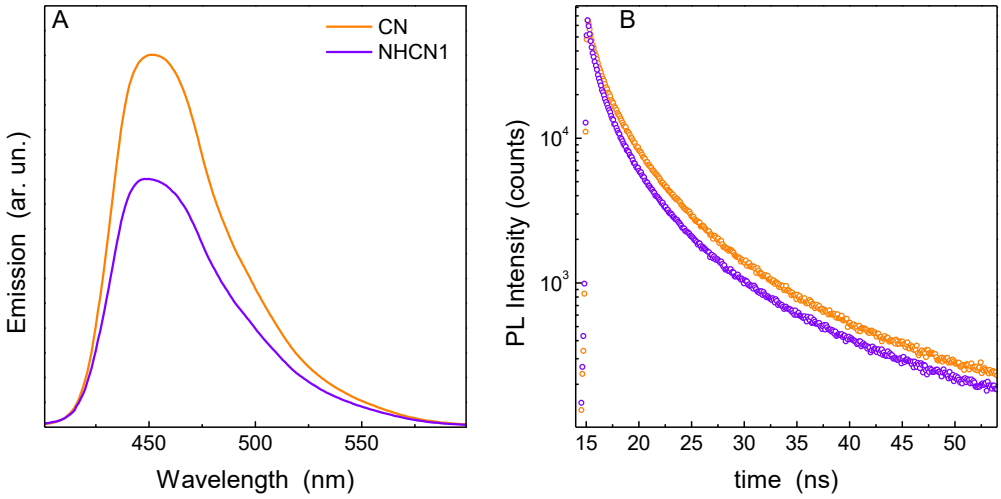

392

393 **Figure 6.** A) Photoluminescence emission spectra of the bare CN and the NHCN1
394 nanocomposite. B) Fluorescence intensity decay curves of the CN and NHCN1 samples. The
395 samples were excited at 404 nm and the emission at 455 nm was collected.

396

397 **4. Conclusions**

398 Herein, we have developed a new class of fully organic photoactive nanocomposites through a
399 simple coupling of carbon nitride (CN) with single-walled carbon nanohorns (CNHs). We

tested the nanocomposites as photocatalysts and established their efficiency for both organic pollutants degradation and photocatalytic H_2 production from water splitting. In the H_2 evolution reaction 1wt.% Pt was used as co-catalyst. Photoactivity in both reactions is greatly affected by the presence of CNHs and is regulated by their content in the nanocomposite. $O_2^{\bullet-}$ species were identified as the main active species responsible for the organic pollutants degradation. The optimized nanocomposite presented a 3-fold increase in photocatalytic H_2 production compared to pristine CN. The enhanced photoactivity was ascribed to the improved charge separation properties as proven by PL and time-resolved fluorescence decay kinetics. We hypothesise that CNHs act as electron acceptors improving charge separation. The present study opens new perspectives in the use of new fully-organic heterostructures in photocatalytic applications.

Acknowledgments: This work was partly supported by the French National Research Agency (ANR) under the program "Make Our Planet Great Again" (ANR-18-MOPGA-0014), the Democritus University of Thrace (project 82268) and the UK Engineering and Physical Sciences Research Council (EP/1508320, EP/N024206/1).

5. References

[1] Y. Ma, X. Wang, Y. Jia, X. Chen, H. Han, C. Li, Titanium dioxide-based nanomaterials for photocatalytic fuel generations, Chem. Rev. 114 (2014) 9987-10043.

[2] K.C. Christoforidis, P. Fornasiero, Photocatalytic hydrogen production: A rift into the future energy supply, ChemCatChem 9 (2017) 1523-1544.

[3] V. Hasija, P. Raizada, A. Sudhaik, K. Sharma, A. Kumar, P. Singh, S.B. Jonnalagadda, V.K. Thakur, Recent advances in noble metal free doped graphitic carbon nitride based nanohybrids for photocatalysis of organic contaminants in water: A review, Appl. Mater. Today, 15 (2019) 494-524.

[4] K.C. Christoforidis, M. Fernández-García, Photoactivity and charge trapping sites in copper and vanadium doped anatase TiO_2 nano-materials, Catal. Sci. Technol., 6 (2016) 1094-1105.

[5] W. Lubitz, W. Tumas, Hydrogen: An Overview, Chem. Rev., 107 (2007) 3900–3903.

[6] Q. Wang, K. Domen, Particulate photocatalysts for light-driven water splitting: mechanisms, challenges, and design strategies, Chem. Rev., 120 (2020) 919–985.

[7] Y.P. Xie, Z.B. Yu, G. Liu, X.L. Ma, H.-M. Cheng, CdS–mesoporous ZnS core–shell particles for efficient and stable photocatalytic hydrogen evolution under visible light, Energy Environ. Sci., 7 (2014) 1895.

[8] D. Cardenas-Morcoso, A.F. Gualdrón-Reyes, A.B.F. Vitoreti, M. García-Tecedor, S.J. Yoon, M.S.d.l. Fuente, I. Mora-Sero, S. Gimenez, Photocatalytic and photoelectrochemical degradation of organic compounds with all-inorganic metal halide perovskite quantum dots, J. Phys. Chem. Lett., 10 (2019) 630-636.

[9] X. Wang, K. Maeda, A. Thomas, K. Takanabe, G. Xin, J.M. Carlsson, K. Domen, M. Antonietti, A metal-free polymeric photocatalyst for hydrogen production from water under visible light, Nat. Mater., 8 (2009) 76-80.

441 [10] V.S. Vyas, V.W.-h. Lau, B.V. Lotsch, Soft photocatalysis: Organic polymers for solar fuel
442 production, Chem. Mater., 28 (2016) 5191-5204.
443 [11] W.J. Ong, L.L. Tan, Y.H. Ng, S.T. Yong, S.P. Chai, Graphitic carbon nitride ($g\text{-}C_3N_4$)-
444 based photocatalysts for artificial photosynthesis and environmental remediation: Are we a step
445 closer to achieving sustainability?, Chem. Rev., 116 (2016) 7159-7329.
446 [12] K.C. Christoforidis, M. Melchionna, T. Montini, D. Papoulis, E. Stathatos, S. Zafeiratos,
447 E. Kordouli, P. Fornasiero, Solar and visible light photocatalytic enhancement of halloysite
448 nanotubes/$g\text{-}C_3N_4$ heteroarchitectures, RSC Adv., 6 (2016) 86617-86626.
449 [13] A. Crake, K.C. Christoforidis, R. Godin, B. Moss, A. Kafizas, S. Zafeiratos, J.R. Durrant,
450 C. Petit, Titanium dioxide/carbon nitride nanosheet nanocomposites for gas phase CO_2
451 photoreduction under UV-visible irradiation, Appl. Catal. B, 242 (2019) 369-378.
452 [14] K.C. Christoforidis, T. Montini, E. Bontempi, S. Zafeiratos, J.J.D. Jaén, P. Fornasiero,
453 Synthesis and photocatalytic application of visible-light active $\beta\text{-}Fe_2O_3/g\text{-}C_3N_4$ hybrid
454 nanocomposites, Appl. Catal. B, 187 (2016) 171-180.
455 [15] E.M. Dias, K.C. Christoforidis, L. Francàs, C. Petit, Tuning thermally treated graphitic
456 carbon nitride for H_2 evolution and CO_2 photoreduction: The effects of material properties and
457 mid-gap states, ACS Appl. Energy Mater., 1 (2018) 6524-6534.
458 [16] C.-C. Wang, X.-H. Yi, P. Wang, Powerful combination of MOFs and C_3N_4 for enhanced
459 photocatalytic performance, Appl. Catal. B, 247 (2019) 24-48.
460 [17] Y. Wei, Y. Zhu, Y. Jiang, Photocatalytic self-cleaning carbon nitride nanotube intercalated
461 reduced graphene oxide membranes for enhanced water purification, Chem. Eng. J., 356 (2019)
462 915-925.
463 [18] Y. Wang, X. Wang, M. Antonietti, Polymeric graphitic carbon nitride as a heterogeneous
464 organocatalyst: from photochemistry to multipurpose catalysis to sustainable chemistry,
465 Angew. Chem., 51 (2012) 68-89.

[19] Y. Zheng, L. Lin, B. Wang, X. Wang, Graphitic carbon nitride polymers toward sustainable photoredox catalysis, Angew. Chem., 54 (2015) 12868-12884.

[20] Q. Han, B. Wang, Y. Zhao, C. Hu, L. Qu, A graphitic-C_3N_4 "Seaweed" architecture for enhanced hydrogen evolution, Angew. Chem., 54 (2015) 11433-11437.

[21] G. Zhang, G. Li, T. Heil, S. Zafeiratos, F. Lai, A. Savateev, M. Antonietti, X. Wang, Tailoring the grain boundary chemistry of polymeric carbon nitride for enhanced solar hydrogen production and CO_2 reduction, Angew. Chem., 58 (2019) 3433-3437.

[22] P. Yang, H. Ou, Y. Fang, X. Wang, A facile steam reforming strategy to delaminate layered carbon nitride semiconductors for photoredox catalysis, Angew. Chem., 56 (2017) 3992-3996.

[23] B. Chai, J. Yan, C. Wang, Z. Ren, Y. Zhu, Enhanced visible light photocatalytic degradation of Rhodamine B over phosphorus doped graphitic carbon nitride, Appl. Surf. Sci., 391 (2017) 376-383.

[24] K.C. Christoforidis, Z. Syrgiannis, V. La Parola, T. Montini, C. Petit, E. Stathatos, R. Godin, J.R. Durrant, M. Prato, P. Fornasiero, Metal-free dual-phase full organic carbon nanotubes/g-C_3N_4 heteroarchitectures for photocatalytic hydrogen production, Nano Energy, 50 (2018) 468-478.

[25] H.R.S. Abdellatif, G. Zhang, X. Wang, D. Xie, J.T.S. Irvine, J. Ni, C. Ni, Boosting photocatalytic oxidation on graphitic carbon nitride for efficient photocatalysis by heterojunction with graphitic carbon units, Chem. Eng. J., 370 (2019) 875-884.

[26] D.J. Martin, P.J. Reardon, S.J. Moniz, J. Tang, Visible light-driven pure water splitting by a nature-inspired organic semiconductor-based system, J. Am. Chem. Soc., 136 (2014) 12568-12571.

[27] M. Anagnostopoulou, A. Zindrou, T. Cottineau, A. Kafizas, C. Marchal, Y. Deligiannakis, V. Keller, K.C. Christoforidis, MOF-derived defective Co_3O_4 nanosheets in carbon nitride

491 nanocomposites for CO_2 photoreduction and H_2 production, ACS Appl. Mater. Interfaces. 15
492 (2023) 6817–6830.
493 [28] J. Ma, D. Huang, W. Zhang, J. Zou, Y. Kong, J. Zhu, S. Komarneni, Nanocomposite of
494 exfoliated bentonite/g-C_3N_4/Ag_3PO_4 for enhanced visible-light photocatalytic decomposition
495 of Rhodamine B, Chemosphere, 162 (2016) 269-276.
496 [29] W.J. Ong, L.L. Tan, S.P. Chai, S.T. Yong, Graphene oxide as a structure-directing agent
497 for the two-dimensional interface engineering of sandwich-like graphene-g-C_3N_4 hybrid
498 nanostructures with enhanced visible-light photoreduction of CO_2 to methane, Chem.
499 Commun., 51 (2015) 858-861.
500 [30] Y. Li, J. Zhan, L. Huang, H. Xu, H. Li, R. Zhang, S. Wu, Synthesis and photocatalytic
501 activity of a bentonite/g-C_3N_4 composite, RSC Adv., 4 (2014) 11831-11839
502 [31] J. Zhang, M. Zhang, L. Lin, X. Wang, Sol processing of conjugated carbon nitride powders
503 for thin-film fabrication, Angew. Chem., 54 (2015) 6297-6301.
504 [32] Y. Gong, J. Wang, Z. Wei, P. Zhang, H. Li, Y. Wang, Combination of carbon nitride and
505 carbon nanotubes: synergistic catalysts for energy conversion, ChemSusChem, 7 (2014) 2303-
506 2309.
507 [33] Y. Zhao, F. Zhao, X. Wang, C. Xu, Z. Zhang, G. Shi, L. Qu, Graphitic carbon nitride
508 nanoribbons: graphene-assisted formation and synergic function for highly efficient hydrogen
509 evolution, Angew. Chem., 53 (2014) 13934-13939.
510 [34] J. Liu, Y. Liu, N. Liu, Y. Han, X. Zhang, H. Huang, Y. Lifshitz, S-T. Lee, J. Zhong, Z.
511 Kang, Metal-free efficient photocatalyst for stable visible water splitting via a two-electron
512 pathway, Science, 347 (2015) 970-974.
513 [35] S. Fang, Y. Xia, K. Lv, Q. Li, J. Sun, M. Li, Effect of carbon-dots modification on the
514 structure and photocatalytic activity of g-C_3N_4, Appl. Catal. B, 185 (2016) 225-232.

515 [36] H. Sun, G. Zhou, Y. Wang, A. Suvorova, S. Wang, A new metal-free carbon hybrid for
516 enhanced photocatalysis, ACS Appl. Mater. Interfaces, 6 (2014) 16745-16754.
517 [37] H. Dai, S. Zhang, G. Xu, L. Gong, M. Fu, X. Li, S. Lu, C. Zeng, Y. Jiang, Y. Lin, G. Chen,
518 A sensitive arecoline photoelectrochemical sensor based on graphitic carbon nitride nanosheets
519 activated by carbon nanohorns, RSC Adv., 4 (2014) 11099.
520 [38] N. Karousis, I. Suarez-Martinez, C.P. Ewels, N. Tagmatarchis, Structure, Properties,
521 Functionalization, and Applications of Carbon Nanohorns, Chem. Rev., 116 (2016) 4850-4883.
522 [39] M. Melchionna, A. Beltram, T. Montini, M. Monai, L. Nasi, P. Fornasiero, M. Prato,
523 Highly efficient hydrogen production through ethanol photoreforming by a carbon
524 nanocone/Pd@TiO_2 hybrid catalyst, Chem. Commun., 52 (2016) 764-767.
525 [40] M. Melchionna, M.V. Bracamonte, A. Giuliani, L. Nasi, T. Montini, C. Tavagnacco, M.
526 Bonchio, P. Fornasiero, M. Prato, Pd@TiO_2/carbon nanohorn electrocatalysts: reversible CO_2
527 hydrogenation to formic acid, Energy Environ. Sci., 11 (2018) 1571-1580.
528 [41] M. Mamatha Kumari, D. Praveen Kumar, P. Haridoss, V. DurgaKumari, M.V. Shankar,
529 Nanohybrid of titania/carbon nanotubes – nanohorns: A promising photocatalyst for enhanced
530 hydrogen production under solar irradiation, Int. J. Hydrogen Energy., 40 (2015) 1665-1674.
531 [42] M.K. M, J. M, A.J. Berkmans, P. Haridoss, L.R. N, S. M.V, Influence of pre-oxidation,
532 versus post-oxidation of carbon nanohorns in TiO_2 nanohybrid for enhanced photocatalytic
533 hydrogen production, Mater. Res. Bull., 109 (2019) 34-40.
534 [43] N. Ramesh Reddy, M. Mamatha Kumari, M.V. Shankar, K. Raghava Reddy, S. Woo Joo,
535 T.M. Aminabhavi, Photocatalytic hydrogen production from dye contaminated water and
536 electrochemical supercapacitors using carbon nanohorns and TiO_2 nanoflower heterogeneous
537 catalysts, J. Environ. Manage., 277 (2021) 111433.
538 [44] C. Cioffi, S. Campidelli, C. Sooambar, M. Marcaccio, G. Marcolongo, M. Meneghetti, D.
539 Paolucci, F. Paolucci, C. Ehli, G.M.A. Rahman, V. Sgobba, D.M. Guldi, M. Prato, Synthesis,

Characterization, and Photoinduced Electron Transfer in Functionalized Single Wall Carbon Nanohorns, J. Am. Chem. Soc., 129 (2007) 3938-3945.

[45] I.D. Petsalakis, G. Pagona, N. Tagmatarchis, G. Theodorakopoulos, Theoretical study in donor–acceptor carbon nanohorn-based hybrids, Chem. Phys. Lett., 448 (2007) 115-120.

[46] S. Brunauer, P.H. Emmett, E. Teller, Adsorption of gases in multimolecular layers, J. Am. Chem. Soc., 60 (1938) 309-319

[47] W. Ho, Z. Zhang, M. Xu, X. Zhang, X. Wang, Y. Huang, Enhanced visible-light-driven photocatalytic removal of NO: Effect on layer distortion on g-C_3N_4 by H_2 heating, Appl. Catal. B 179 (2015) 106-112.

[48] T. Azami, D. Kasuya, R. Yuge, M. Yudasaka, S. Iijima, T. Yoshitake, Y. Kubo, Large-scale production of single-wall carbon nanohorns with high purity, J. Phys. Chem. C, 112 (2008) 1330-1334.

[49] S. Battiston, M. Minella, R. Gerbasi, F. Visentin, P. Guerriero, A. Leto, G. Pezzotti, E. Miorin, M. Fabrizio, C. Pagura, Growth of titanium dioxide nanopetals induced by single wall carbon nanohorns, Carbon, 48 (2010) 2470-2477.

[50] S. Battiston, M. Bolzan, S. Fiameni, R. Gerbasi, M. Meneghetti, E. Miorin, C. Mortalò, C. Pagura, Single wall carbon nanohorns coated with anatase titanium oxide, Carbon, 47 (2009) 1321-1326.

[51] L. Zhao, X. Chen, X. Wang, Y. Zhang, W. Wei, Y. Sun, M. Antonietti, M.M. Titirici, One-step solvothermal synthesis of a carbon@TiO_2 dyade structure effectively promoting visible-light photocatalysis, Adv. Mater., 22 (2010) 3317-3321.

[52] X. Liu, N. Chen, Y. Li, D. Deng, X. Xing, Y. Wang, A general nonaqueous sol-gel route to g-C3N4-coupling photocatalysts: the case of Z-scheme g-C_3N_4/TiO_2 with enhanced photodegradation toward RhB under visible-light, Sci. Rep., 6 (2016) 39531.

564 [53] Z. Zhao, Y. Sun, Q. Luo, F. Dong, H. Li, W.-K. Ho, Mass-controlled direct synthesis of
565 graphene-like carbon nitride nanosheets with exceptional high visible light activity. Less is
566 better, Sci. Rep., 5 (2015) 14643.
567 [54] J. Moon, C.Y. Yun, K.-W. Chung, M.-S. Kang, J. Yi, Photocatalytic activation of TiO_2
568 under visible light using Acid Red 44, Catal. Today, 87 (2003) 77-86.
569 [55] C. Zhou, D. Huang, P. Xu, G. Zeng, J. Huang, T. Shi, C. Lai, C. Zhang, M. Cheng, Y. Lu,
570 A. Duan, W. Xiong, M. Zhou, Efficient visible light driven degradation of sulfamethazine and
571 tetracycline by salicylic acid modified polymeric carbon nitride via charge transfer, Chem. Eng.
572 J., 370 (2019) 1077-1086.
573 [56] C. Zhou, P. Xu, C. Lai, C. Zhang, G. Zeng, D. Huang, M. Cheng, L. Hu, W. Xiong, X.
574 Wen, L. Qin, J. Yuan, W. Wang, Rational design of graphic carbon nitride copolymers by
575 molecular doping for visible-light-driven degradation of aqueous sulfamethazine and hydrogen
576 evolution, Chem. Eng. J., 359 (2019) 186-196.
577 [57] K.C. Christoforidis, I.A. Vasiliadou, M. Louloudi, Y. Deligiannakis, Gallic acid mediated
578 oxidation of pentachlorophenol by the Fenton reaction under mild oxidative conditions, J.
579 Chem. Technol. Biotechnol., 93 (2018) 1601-1610.
580 [58] M. Shalom, S. Inal, C. Fettkenhauer, D. Neher, M. Antonietti, Improving carbon nitride
581 photocatalysis by supramolecular preorganization of monomers, J. Am. Chem. Soc., 135
582 (2013) 7118-7121.
583 [59] Z. Zhang, K. Liu, Z. Feng, Y. Bao, B. Dong, Hierarchical sheet-on-sheet $ZnIn_2S_4$/g-C_3N_4
584 heterostructure with highly efficient photocatalytic H_2 production based on photoinduced
585 interfacial charge transfer, Sci. Rep., 6 (2016) 19221.
586 [60] H. Wang, X. Sun, D. Li, X. Zhang, S. Chen, W. Shao, Y. Tian, Y. Xie, Boosting hot-
587 electron generation: exciton dissociation at the order-disorder interfaces in polymeric
588 photocatalysts, J. Am. Chem. Soc., 139 (2017) 2468-2473.

589 [61] G. Zhang, G. Li, Z.A. Lan, L. Lin, A. Savateev, T. Heil, S. Zafeiratos, X. Wang, M.
590 Antonietti, Optimizing optical absorption, exciton dissociation, and charge transfer of a
591 polymeric carbon nitride with ultrahigh solar hydrogen production activity, Angew. Chem., 56
592 (2017) 13445-13449.
593 [62] Y. Guo, J. Li, Y. Yuan, L. Li, M. Zhang, C. Zhou, Z. Lin, A rapid microwave-assisted
594 thermolysis route to highly crystalline carbon nitrides for efficient hydrogen generation,
595 Angew. Chem., 55 (2016) 14693-14697.
596 [63] G. Pagona, A.S.D. Sandanayaka, T. Hasobe, G. Charalambidis, A.G. Coutsolelos, M.
597 Yudasaka, S. Iijima, N. Tagmatarchis, Characterization and photoelectrochemical properties
598 of nanostructured thin film composed of carbon nanohorns covalently functionalized with
599 porphyrins, J. Phys. Chem. C, 112 (2008) 15735-15741.
600